

# Exchange bias effect in martensitic epitaxial Ni-Mn-Sn thin films applied to pin CoFeB/MgO/CoFeB magnetic tunnel junctions

N. Teichert,<sup>1, a)</sup> A. Boehnke,<sup>1</sup> A. Behler,<sup>2</sup> B. Weise,<sup>2</sup> A. Waske,<sup>2</sup> and A. Hütten<sup>1</sup>

<sup>1)</sup>Department of Physics, Center for Spinelectronic Materials and Devices, Bielefeld University, 33615 Bielefeld, Germany

<sup>2)</sup>IFW Dresden, Institute for Complex Materials, P.O. Box 27 01 16, 01171 Dresden, Germany

(Dated: 7 December 2024)

The exchange bias effect is commonly used to shift the coercive field of a ferromagnet. This technique is crucial for the use of magnetic tunnel junctions as logic or memory devices. Therefore, an independent switching of the two ferromagnetic electrodes is necessary to guarantee a reliable readout. Here, we demonstrate that the intrinsic exchange bias effect of Ni-Mn-Sn can be used to apply a unidirectional anisotropy to magnetic tunnel junctions. For this, we use epitaxial Ni-Mn-Sn films as pinning layers for microfabricated CoFeB/MgO/CoFeB magnetic tunnel junctions. We compare the exchange bias field ( $H_{EB}$ ) measured after field cooling in  $-10$  kOe external field by magnetization measurements with  $H_{EB}$  obtained from tunnel magnetoresistance measurements. For both methods we find the same magnitude and temperature dependence of  $H_{EB}$ .

PACS numbers: 81.30.Kf, 75.70.-i, 75.30.Et, 85.30.Mn

The exchange bias effect (EB) describes a unidirectional magnetic anisotropy resulting in a shift of the magnetic hysteresis along the direction of the applied field.<sup>1</sup> It is observed in structures with interfaces between ferromagnetic (FM) and antiferromagnetic (AF) phases, e.g. thin film structures with FM and AF layers.<sup>2</sup> EB is commonly used to pin magnetic electrodes in magnetic tunnel junctions (MTJs). The magnetic shape memory Heusler compounds Ni-Mn-X (X= Sn, In, Sb) show an intrinsic EB in the martensitic state at low temperature caused by FM and AF regions in the material.<sup>3-6</sup> Accordingly, these compounds are promising candidates for pinning ferromagnetic electrodes of MTJs without the commonly used antiferromagnets, MnIr and MnPt.<sup>7-9</sup> Replacing these materials in industrial applications is desirable because of the rarity and high cost of Iridium and Platinum. Here, we present how Ni-Mn-Sn thin films can serve as pinning layer in CoFeB/MgO/CoFeB MTJs and thus, show the technological applicability of the EB of Ni-Mn-X Heusler compounds. Since Ni-Mn-Sn is magnetic and shows an intrinsic EB, in principle it could serve as pinning layer and magnetic electrode at once. Nevertheless, we use CoFeB electrodes because they are well established<sup>10</sup> and the spin-polarization of Ni-Mn-Sn is small which is unfavorable for electrodes in MTJs.<sup>11</sup>

The samples were fabricated by magnetron sputtering and subsequent e-beam lithography. In a first step we deposit the 220 nm thick Ni-Mn-Sn layer on MgO(001) substrates by co-sputtering from elemental targets as described in Ref. 12. The substrate temperature during the deposition was 650°C. After the deposition process the samples are cooled to room temperature and the additional layers Co<sub>40</sub>Fe<sub>40</sub>B<sub>20</sub>/MgO/Co<sub>40</sub>Fe<sub>40</sub>B<sub>20</sub>/Ta/Ru

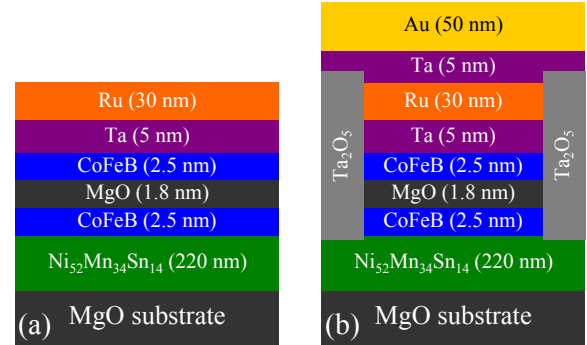


FIG. 1. Sketches of the layer system: a) as deposited, and b) after annealing and nanofabrication.

were deposited with film thicknesses as shown in Fig. 1a. Using these "as deposited" samples, the magnetization measurements were conducted.

In order to prepare the MTJs for tunnel magnetoresistance (TMR) measurements the deposited layer stacks annealed at 350°C for one hour for proper crystallization of the CoFeB electrodes.<sup>13</sup> Afterwards ellipsoidal MTJs (240 nm x 320 nm) were patterned out of the layer stack by e-beam lithography and subsequent Ar ion milling. The ion milling was stopped right below the lower CoFeB layer in order to keep the Ni-Mn-Sn film intact. This is necessary because the crystallite size of shape memory materials has a high impact on the transformation characteristics and the martensitic transformation can be impeded in too small crystals.<sup>14-16</sup> The MTJs were insulated by Ta<sub>2</sub>O<sub>5</sub> and equipped with Ta/Au contact pads by RF and DC magnetron sputtering. The final layer structure is sketched in Fig. 1b.

Composition and epitaxial growth of the Ni-Mn-Sn layer were checked by energy dispersive X-ray spec-

<sup>a)</sup>Electronic mail: nteichert@physik.uni-bielefeld.de

troscopy and X-ray diffraction measurements, respectively. The film thickness of the individual layers was examined by X-ray reflectivity measurements. The magnetization was studied using a vibrating sample magnetometer (Quantum Design PPMS) with in-plane applied magnetic field. TMR was measured using common 2-probe method with a constant 100 mV DC bias voltage and a Cryogenic He cryostat system where the external field is applied along the major axis of the ellipsoidal MTJs.

In order to determine the magnetic properties and martensitic transformation of the Ni-Mn-Sn the temperature dependence of the magnetization was studied. The magnetization values given in the paper are the measured magnetic moments normalized with the total volume of magnetic material (film area  $\times$  225 nm). The magnetization versus temperature for the "as deposited" sample in field cooling (FC) and field heating (FH), and during heating after cooling in zero magnetic field (ZFC) measured in low external field is shown in Fig. 2a. The distinct drop of the magnetization upon cooling results from the martensitic transformation. For Ni-Mn-Sn, the magnetization of martensite is lower than that of austenite. The reason for the magnetization change is a change in the alignment of magnetic moments of the Mn atoms on Mn sites ( $Mn_1$ ) and Mn atoms on Sn sites ( $Mn_2$ ) which are known to couple antiferromagnetically in austenite and martensite. However, due to changed lattice constants the antiferromagnetic coupling between  $Mn_1$  and  $Mn_2$  is strengthened in the martensite.<sup>17-19</sup> The martensitic transformation temperature and Curie temperature of the Ni-Mn-Sn are  $T_M = 256$  K and  $T_C = 317$  K, respectively, determined from inflection points of the FC magnetization curve. Above  $T_C$  the magnetization drops to  $27 \text{ emu cm}^{-3}$ . This remaining magnetization results from the CoFeB, which has a higher Curie temperature. The splitting between the ZFC and FC curve originates from the coexistence of ferromagnetic and antiferromagnetic regions at low temperatures in the martensite phase, which is the basis for the EB.<sup>20,21</sup>

Commonly, the intrinsic EB in Ni-Mn-Sn is determined via isothermal magnetization curves at low temperature after cooling the specimen in an external magnetic field. Fig. 2b-d depict the magnetic hysteresis loops after field cooling the sample to 10 K in -10 kOe external field. At 10 K it is clearly visible that at low temperatures the magnetic hysteresis is shifted and the positive coercive field  $H_{c1}$  is larger than the negative coercive field  $H_{c2}$ . The exchange bias field is defined as  $H_{EB} = (H_{c1} + H_{c2})/2$ . At 80 K (Fig. 2c) the curve is symmetric and  $H_{EB} = 0$ . Above  $T_c$  a small magnetic hysteresis of the CoFeB ( $H_c = 5$  Oe) is visible, as exhibited in Fig. 2d. The saturation magnetization of CoFeB appears to be small, because the magnetic moment is normalized using a film thickness of 225 nm as described above. Below  $T_c$  the contribution of CoFeB to the measured magnetization is small and the magnitudes of the

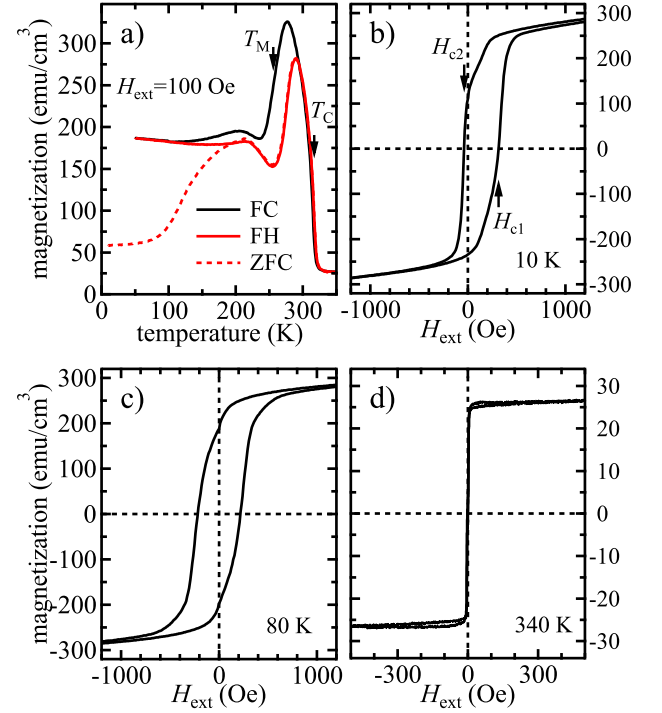


FIG. 2. Magnetization measurements of the "as deposited" layer stack (cf. Fig. 1a): a)  $M(T)$  curves at 100 Oe applied field. The FC and FH curves envelop a thermal hysteresis due to the martensitic transition. The FH and ZFC curves are split at low temperature. The martensitic transformation temperature  $T_M$  and Curie temperature  $T_C$  of Ni-Mn-Sn are indicated by arrows. b)-d)  $M(H)$  curves after field cooling at -10 kOe. The EB leads to a shift of  $H_{c1}$  and  $H_{c2}$  in positive field direction at low temperature.

determined  $H_{EB}$  and  $H_c$  represent the values for Ni-Mn-Sn and are not significantly influenced by the magnetic moments of the two 2.5 nm thin CoFeB layers.

In the following, the EB is determined from TMR measurements of MTJs patterned out of the layers on top of the Ni-Mn-Sn. Fig. 3 shows the TMR ratio defined as  $TMR = (R - R_p)/R_p$  versus external field.  $R_p$  denotes the resistance at parallel alignment of both CoFeB electrodes, i.e. the resistance at high applied field. Hereby, the EB is defined as  $H_{EB}^{TMR} = (H_{m1} + H_{m2})/2$  and deduced from  $H_{m1}$  and  $H_{m2}$  which denote the external fields of maximum TMR in increasing and decreasing field, respectively. At temperatures up to  $T_c$  (Fig. 3a-e) the TMR curves are highly asymmetric and the resistivity change occurs in multiple steps. Above  $T_c$  when only the CoFeB is ferromagnetic, the TMR curves are symmetric and the resistivity change occurs abrupt (cf. Fig. 3f) as expected for unpinned CoFeB/MgO/CoFeB MTJs.<sup>10</sup> Here, the maximum TMR is obtained for  $H_{ext} = 0$  which means that the CoFeB electrodes couple antiferromagnetically. This can be explained by magnetostatic coupling of the CoFeB layers induced by uncompensated magnetic poles at the edges of the electrodes.<sup>22</sup> Below  $T_c$

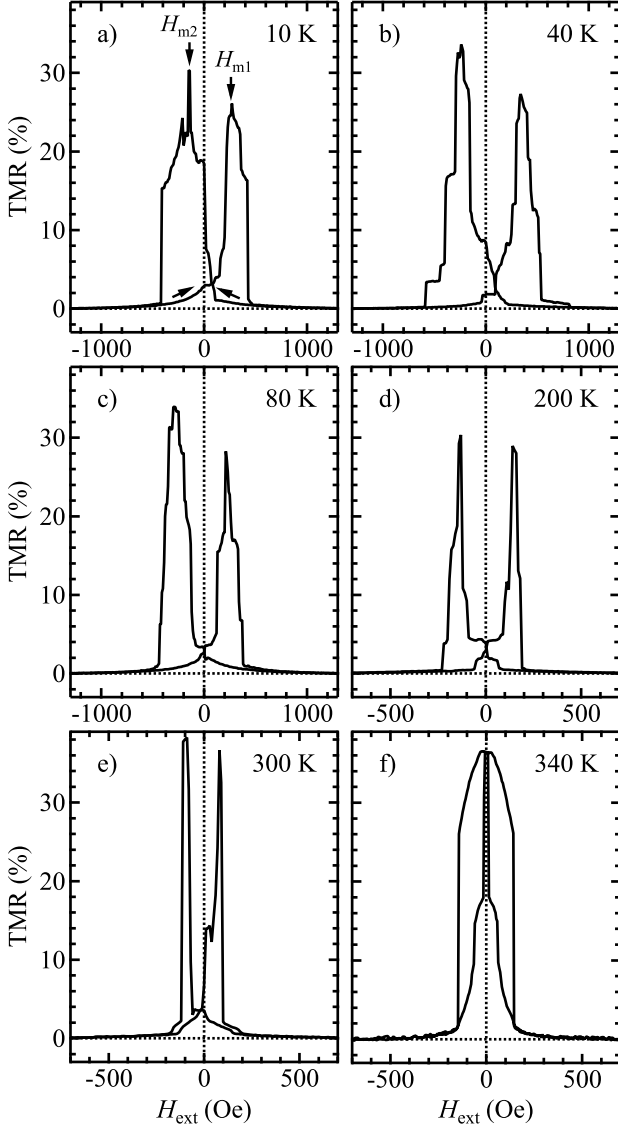


FIG. 3. TMR curves at 100 mV bias voltage after field cooling at -10 kOe. At low temperature the EB is visible (a and b). f) shows the TMR for paramagnetic Ni-Mn-Sn where the TMR curve is symmetric and magnetic switching is sharp.

the magnetic switching of the bottom CoFeB electrode is determined by the domain structure of the much thicker Ni-Mn-Sn layer. The domains of the Ni-Mn-Sn are probably smaller than the MTJs and not significantly influenced by adjacent CoFeB. However, the bottom CoFeB layer adopts the domain structure from the Ni-Mn-Sn layer below  $T_c$  since both layers are in direct contact. Furthermore, the stray field from the Ni-Mn-Sn domains affect the domain structure of the top CoFeB electrode. Above  $T_c$  the influence of Ni-Mn-Sn is not present and the CoFeB electrodes switch abruptly and symmetrically. However, at low temperatures (Fig. 3a and b) a shift of the maxima of the TMR curves in positive field direction is clearly visible and the EB can be observed. The

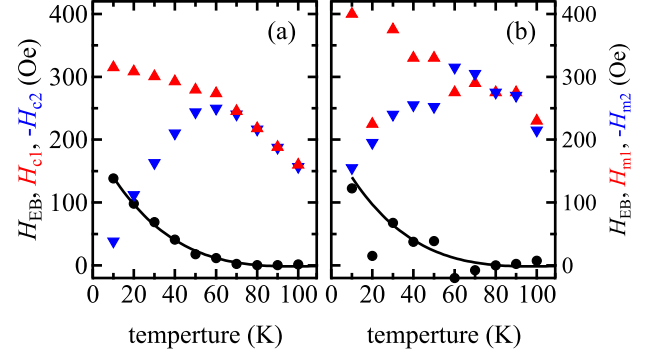


FIG. 4. Temperature dependence of the EB after field cooling at -10 kOe. a)  $H_{c1}$ ,  $H_{c2}$ , and  $H_{EB}$  determined from magnetization measurements. The black line is a guide to the eye and identical in a and b. b)  $H_{m1}$ ,  $H_{m2}$ , and  $H_{EB}$  determined from TMR curves.

TMR amplitude fluctuates between 25% and 38% and does not show a significant temperature dependence. It needs to be stated that the MTJ layer stack is not optimized by means of film thicknesses and selection of the optimum materials for the magnetic electrodes and the tunnel barrier in order to obtain maximum TMR. This will be a subject of future work.

The temperature dependence of the EB is depicted in Fig. 4 where both methods of determining EB are compared. Fig. 4a shows  $H_{c1}$ ,  $H_{c2}$ , and  $H_{EB}$  as determined by magnetization measurements. At low temperature  $|H_{c1}|$  and  $|H_{c2}|$  are different. With increasing temperature  $|H_{c2}|$  strongly increases while  $|H_{c1}|$  mildly decreases up to 60 K. Above 70 K the values of positive and negative coercive fields are equal and decrease with increasing temperature. Accordingly,  $H_{EB}$  strongly decreases with increasing temperature from  $H_{EB} = 138$  Oe at 10 K to zero above 70 K. The magnitude and temperature dependence of  $H_{EB}$  is comparable to bulk Ni-Mn-Sn.<sup>3,23</sup> Fig. 4b depicts the corresponding results from TMR measurements. The depicted data are average values obtained from TMR curves of two different MTJs measured during the first and second field loop at each temperature point.  $H_{m1}$  and  $H_{m2}$  show the same trends as  $H_{c1}$  and  $H_{c2}$ . The measured TMR curves and the exact positions of  $H_{m1}$  and  $H_{m2}$  are not identical because of the influence of magnetic domains in Ni-Mn-Sn below  $T_c$ . This random influence can be of the same order of magnitude as the exchange bias which leads to a very small  $H_{EB}$  at 20 K and a negative  $H_{EB}$  at 60 K. Nevertheless, it is clearly visible from Fig. 4a and b that  $H_{EB}$  has the same magnitude and temperature dependence. So, the intrinsic EB of Ni-Mn-Sn can be observed in TMR measurements.

In summary, we investigated the exchange bias effect of a Ni-Mn-Sn/CoFeB/MgO/CoFeB thin film structure after field cooling by two different methods: direct magnetization measurements and TMR measurements. Magnetization measurements are used to quantify the intrinsic EB of the Ni-Mn-Sn layer while the influence of the

magnetic moment of the thin CoFeB layers is negligible. TMR measurements, however, are sensitive to the interaction between the Ni-Mn-Sn layer and the CoFeB tunnel electrodes. Since we have shown a comparable EB effect in MTJs and magnetization measurements, we conclude that epitaxial Ni-Mn-Sn thin films can serve as pinning layers in these devices.

## ACKNOWLEDGMENTS

The authors gratefully acknowledge funding by the DFG through SPP 1599 “Ferroic Cooling”. Collaboration with the European-Japanese FP7 project HARFIR is gratefully acknowledged.

- <sup>1</sup>W. Meiklejohn and C. Bean, *Phys. Rev.* **102**, 1413 (1956).
- <sup>2</sup>J. Nogues and I. Schuller, *J. Magn. Magn. Mater.* **192**, 203 (1999).
- <sup>3</sup>M. Khan, S. Stadler, and N. Ali, *J. Appl. Phys.* **102**, 113914 (2007).
- <sup>4</sup>M. Khan, I. Dubenko, S. Stadler, and N. Ali, *Appl. Phys. Lett.* **91**, 072510 (2007).
- <sup>5</sup>A. K. Pathak, M. Khan, B. R. Gautam, S. Stadler, I. Dubenko, and N. Ali, *J. Magn. Magn. Mater.* **321**, 963 (2009).
- <sup>6</sup>R. Machavarapu and G. Jakob, *Appl. Phys. Lett.* **102**, 232406 (2013).
- <sup>7</sup>S. Kämmerer, A. Thomas, A. Hütten, G. Reiss, *Appl. Phys. Lett.* **85**, 79 (2004).
- <sup>8</sup>Y. M. Lee, J. Hayakawa, S. Ikeda, F. Matsukura, and H. Ohno, *Appl. Phys. Lett.* **89**, 042506 (2006).
- <sup>9</sup>J. M. Teixeira, J. Ventura, M. P. Fernandez-Garcia, J. P. Araujo, J. B. Sousa, P. Wisniewski, D. C. Leitao, and P. P. Freitas, *J. Appl. Phys.* **111**, 053930 (2012).
- <sup>10</sup>S. Ikeda, J. Hayakawa, Y. Ashizawa, Y. M. Lee, K. Miura, H. Hasegawa, M. Tsunoda, F. Matsukura, and H. Ohno, *Appl. Phys. Lett.* **93**, 082508 (2008).
- <sup>11</sup>M. Ye, A. Kimura, Y. Miura, M. Shirai, Y. T. Cui, K. Shimada, H. Namatame, M. Taniguchi, S. Ueda, K. Kobayashi, R. Kainuma, T. Shishido, K. Fukushima, and T. Kanomata, *Phys. Rev. Lett.* **104**, 176401 (2010).
- <sup>12</sup>A. Auge, N. Teichert, M. Meinert, G. Reiss, A. Hütten, E. Yüzüak, I. Dincer, Y. Elerman, I. Ennen, and P. Schattschneider, *Phys. Rev. B* **85**, 214118 (2012).
- <sup>13</sup>J. Schmalhorst, A. Thomas, G. Reiss, X. Kou, E. Arenholz, J. Appl. Phys. **102**, 053907 (2007).
- <sup>14</sup>N. Teichert, A. Auge, E. Yüzüak, I. Dincer, Y. Elerman, B. Krumme, H. Wende, O. Yildirim, K. Potzger and A. Hütten, *Acta Mater.* **86**, 279 (2015).
- <sup>15</sup>Q. Meng, Y. Rong, T. Y. Hsu, *Phys. Rev. B* **65**, 174118 (2002).
- <sup>16</sup>G. A. Malygin, *Tech. Phys.* **54**, 1782 (2009).
- <sup>17</sup>S. Aksoy, M. Acet, P. P. Deen, L. Mañosa, and A. Planes, *Phys. Rev. B* **79**, 212401 (2009).
- <sup>18</sup>V. V. Sokolovskiy, V. D. Buchelnikov, M. A. Zagrebin, P. Entel, S. Sahoo, and M. Ogura, *Phys. Rev. B* **86**, 134418 (2012).
- <sup>19</sup>A. Behler, N. Teichert, B. Dutta, A. Waske, T. Hickel, A. Auge, A. Hütten, and J. Eckert, *AIP Adv.* **3** 122112 (2009).
- <sup>20</sup>T. Krenke, M. Acet, E. F. Wassermann, X. Moya, L. Manosa, and A. Planes, *Phys. Rev. B* **72**, 014412 (2005).
- <sup>21</sup>B. M. Wang, Y. Liu, P. Ren, B. Xia, K. B. Ruan, J. B. Yi, J. Ding, X. G. Li, and L. Wang, *Phys. Rev. Lett.* **106**, 077203 (2011).
- <sup>22</sup>A. Anguelouch, B. D. Schrag, G. Xiao, Y. Lu, P. L. Trouilloud, R. A. Wanner, W. J. Gallagher, and S. S. P. Parkin, *Appl. Phys. Lett.* **76**, 622 (2000).
- <sup>23</sup>Z. Li, C. Jing, J. Chen, S. Yuan, S. Cao, and J. Zhang, *Appl. Phys. Lett.* **91**, 112505 (2007).